Available online at www.sciencedirect.com
ScienceDirect
Journal of Sound and Vibration 322 (2009) 772–784
JOURNAL OF SOUND AND VIBRATION
www.elsevier.com/locate/jsvi

On self-noise at the nose of a supercavitating vehicle

M.S. Howe[a,*], A.M. Colgan[a], T.A. Brungart[b]

[a]*College of Engineering, Boston University, 110 Cummington Street, Boston, MA 02215, USA*
[b]*Applied Research Laboratory, The Pennsylvania State University, State College, PA 16804, USA*

Received 20 March 2008; received in revised form 8 November 2008; accepted 13 November 2008
Handling Editor: P. Joseph
Available online 23 December 2008

Abstract

The cavity of a supercavitating vehicle in water is maintained by the steady injection of gas from sources within the vehicle and cavity. An analysis is made in this paper to estimate the spectrum of the acoustic 'self-noise' produced at the nose of the vehicle by the unsteady impingement of the gas on the cavity interface. For the purposes of calculation it is assumed that the supercavity is circular cylindrical and is formed to the rear of a hemispherical cavitator. This arrangement closely approximates a supercavity being investigated experimentally at the Penn State Applied Research Laboratory. A 'transfer function' is derived for this configuration that relates the self-noise pressure at the nose to the pressure distribution on the cavity wall attributable to the impinging gas. It is applicable also to any geometrically similar supercavity maintained by gas injection, provided that the distribution on the interface of the surface pressure spectrum of fluctuations produced by the impinging gas is known. Numerical results are given using experimental data for the cavity wall surface pressure produced by a narrow, impinging air jet and when the nose is acoustically hard, but the method is easily modified to deal with more general impedance conditions on the cavitator.

1. Introduction

A supercavitating underwater vehicle attains high forward speeds because of the great reduction in the drag obtained by enclosing most of the length of the vehicle within a *ventilated supercavity*. The cavity is formed at a 'cavitator' near the vehicle nose [1–3], and maintained in a stable form by the carefully controlled injection of gas from sources near the cavitator [4,5]. Vehicle guidance may be achieved by the use of high-frequency acoustic sensors situated within the nose. Turbulence and instabilities of the gas–water interface are sources of unwanted 'hydrodynamic sound' [6–11] that can interfere with the operation of these sensors. However, an important additional contribution to this noise has been attributed to the direct impingement of the ventilating gas (delivered at relatively high speed from inlet nozzles) on the cavity interface [12–14].

The production of sound by gas-jet impingement on the interface has been examined experimentally at the Applied Research Laboratory (ARL) of Penn State University using the supercavitating vehicle model illustrated schematically in Fig. 1. The ventilating gas enters the cavity axisymmetrically through 20 radially

*Corresponding author.
E-mail address: mshowe@bu.edu (M.S. Howe).

0022-460X/$ - see front matter © 2008 Elsevier Ltd. All rights reserved.
doi:10.1016/j.jsv.2008.11.019

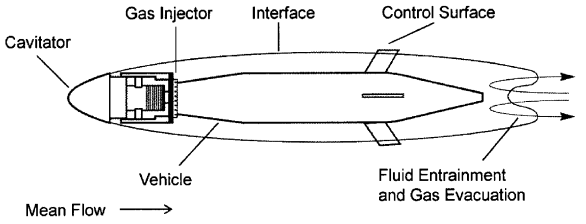

Fig. 1. Schematic of the ARL experimental supercavity.

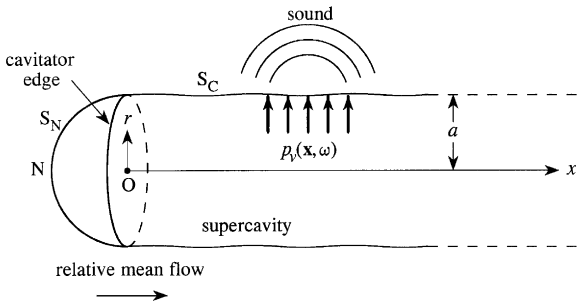

Fig. 2. Supercavity model with a hemispherical cavitator of radius a used to estimate the sound pressure produced at the nose N by the impingement of ventilating gas on the gas–water interface with surface pressure $p_v(\mathbf{x},\omega)$.

orientated nozzles equally spaced circumferentially on a 'gas injector ring' just aft of the cavitator. In this arrangement the jet impingement velocity on the interface is typically $\sim$50 m/s at close to normal incidence. The destruction of jet momentum at the interface results in the production of sound in the water of *dipole* type, the dipole axis being in the direction of the local interface normal. Each jet is turbulent and produces broad-spectrum sound that tends to radiate directly away from the interface at high frequencies [13,14]. Direct radiation towards the nose is inhibited by the fact that, for water-borne sound, the interface may in a first approximation be regarded as a pressure release surface.

However, it is important to be able to quantify the influence of these jet dipoles (and other surface related sound sources) on the sound measured at the vehicle nose. The purpose of this paper is to provide analytical estimates of this in the form of a frequency dependent *transfer function*. This can be done with relative ease and to a sufficient approximation for the simplified geometry shown in Fig. 2, where the nose shape is assumed to be a hemisphere and the cavity interface is replaced by a circular cylinder of the same radius as the nose. Approximate formulae for the sound level at the nose will be developed at high, low and intermediate frequencies. The calculations must take explicit account of nose diffraction at high frequencies, and in all cases account must also be taken of the surface 'hard/pressure-release' transition that occurs at the trailing edge of the cavitator.

The mathematical problem is formulated in Section 2. The diffraction formulae at high and low frequencies are obtained in Sections 3 and 4. These are used in Section 5 to derive a composite estimate of the transfer function over all relevant frequencies. Early test data taken from the literature for a single impinging gas jet are used to make a sample prediction of the self-noise at the nose.

2. Representation of the self-noise at the nose

The undisturbed position of the gas–water interface (S_C in Fig. 2) is assumed to coincide with a circular cylinder coaxial with the positive x-axis and of radius $r = a$, where the coordinate origin is taken at the midpoint O of the rear, plane face of the idealized hemispherical cavitator. The water has density ρ_o and sound speed c_o, and the Mach number of the relative mean flow of water over the supercavity is sufficiently small that the convection of sound can be ignored. Therefore, when contributions from extraneous turbulence noise

sources within the water are neglected, small amplitude pressure fluctuations $p(\mathbf{x},\omega)\,\mathrm{e}^{-\mathrm{i}\omega t}$ of radian frequency ω (where t denotes time) propagate within the water according to [6–11]

$$(\nabla^2 + k_o^2)p = 0, \tag{1}$$

where $k_o = \omega/c_o$ is the acoustic wavenumber. The visco-thermal dissipation of the sound is ignored, so that the condition of impermeability implies that $\partial p/\partial x_n = 0$ on the surface S_N of the cavitator, where x_n denotes a local normal coordinate directed into the water.

We consider the sound generated in the water by the impingement of ventilating gas on the cavity wall S_C. This produces a distributed fluctuating surface pressure $p_v(\mathbf{x},\omega)$ on the interior face of the interface that is acoustically equivalent to a distribution of dipole sources radiating into the water. It is assumed that $p_v(\mathbf{x},\omega)$ is known from measurement or from previous numerical simulation. Because of the very large differences in the mean gas and water densities it is also assumed in a first approximation that the pressure p vanishes elsewhere on the cavity interface.

Let $p_\mathrm{N}(\omega)$ denote the unsteady pressure produced by this mechanism on the hemispherical surface S_N of the cavitator at the nose, i.e. at the point of intersection of the negative x-axis and S_N. It is expressed in terms of $p_v(\mathbf{x},\omega)$ by introducing a Green's function $G(\mathbf{x},\omega)$ that is the solution with outgoing wave behaviour of

$$(\nabla^2 + k_o^2)G = 0 \tag{2}$$

in the water, subject to

$$\left.\begin{array}{ll} \partial G/\partial x_n = \delta(y)\delta(z) & \text{on } S_\mathrm{N} \\ G = 0 & \text{on } S_\mathrm{C} \end{array}\right\}, \tag{3}$$

where the coordinates y, z are defined such that $\mathbf{x} = (x, y, z)$ forms a conventional rectangular, right-handed system. It is clear that this definition implies that G is axisymmetric with respect to the axis of the supercavity, i.e. that $G \equiv G(x, r, \omega)$ where $r = \sqrt{y^2 + z^2}$.

The application of Green's theorem and the radiation condition to Eqs. (1), (2) yields [10,15–17]

$$\oint_{S_\mathrm{N}+S_\mathrm{C}} \left(p(\mathbf{x},\omega)\frac{\partial G}{\partial x_n}(\mathbf{x},\omega) - G(\mathbf{x},\omega)\frac{\partial p}{\partial x_n}(\mathbf{x},\omega)\right)\mathrm{d}S = 0, \tag{4}$$

where the integration is over the combined surfaces $S_\mathrm{N} + S_\mathrm{C}$ of the cavitator and the cavity interface. The second term in the integrand vanishes identically, because $\partial p/\partial x_n = 0$ on S_N and $G = 0$ on S_C. The condition that $p \equiv p_v$ on S_C and the first of conditions (3) then supply

$$p_\mathrm{N}(\omega) = \int_S p_v(\mathbf{x},\omega)T(x,\omega)\,\mathrm{d}S, \tag{5}$$

where the integration is over the impingement region S, say, of the cavity interface, and where

$$T(x,\omega) \equiv -\left(\frac{\partial G}{\partial r}(x,r,\omega)\right)_{r=a}. \tag{6}$$

The determination of the 'self-noise' is accordingly reduced to the resolution of the reciprocal problem of finding the frequency dependence of the (axisymmetric) *transfer function* $T(x,\omega)$ on S_C at distance x from the edge of the cavitator. It is clear that this function must be axisymmetric and dependent only on the distance x from the cavitator; indeed symmetry demands that the pressure produced at the nose by a pressure loading $p_v(\mathbf{x},\omega)$ applied at a *point* on S_C can depend only on the axial distance x and not on the azimuthal location of the point of application.

3. The transfer function at high frequencies

At very high frequencies, such that $k_o a \gg 1$, the impingement region S on the cavity interface lies in the 'acoustic shadow' of the direct radiation from the point source at the nose (Fig. 3). The asymptotic behaviour of the Green's function in this shadow region will be estimated by surface wave diffraction theory (see, e.g. Refs. [18–26]). This is done in two stages. First, we calculate the surface diffracted waves propagating over the

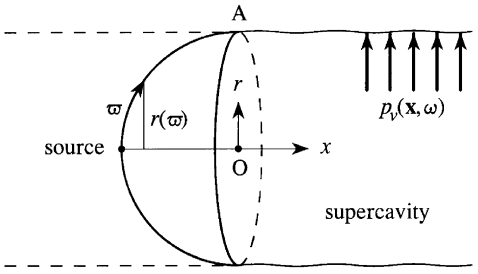

Fig. 3. Configuration used to calculate the transfer function from the solution of the wave equation representing the motion produced in the water by a unit point source at the nose.

hemispherical cavitator and incident on the edge A. Second, the secondary diffraction of these waves at the edge A is calculated.

3.1. Surface diffracted waves

The surface diffraction of high-frequency waves from the source leads to a well known representation in terms of 'creeping modes' and it is only necessary to give here a minimum of details necessary for the present discussion.

Temporarily take the origin at the source. The source field is axisymmetric, and the mathematical description of high-frequency propagation *near* the surface of the cavitator can then be simplified by introduction of local coordinates (x_n, ϖ), where x_n denotes distance in the normal direction from the cavitator into the fluid, and ϖ denotes curvilinear distance measured on the surface from the source along a 'great circle'. Green's function can depend only on x_n, ϖ, because the motion is axisymmetric. At high frequencies and close to the surface where $x_n \ll a$, we write $G \equiv G_N$, where G_N may be taken to satisfy the following 'earth flattening' approximation to the wave equation [20–25]

$$\left[\frac{\partial^2}{\partial x_n^2} + \left(1 - \frac{2x_n}{a}\right)\frac{1}{\varpi}\frac{\partial}{\partial \varpi}\left(\varpi \frac{\partial}{\partial \varpi}\right) + k_o^2\right] G_N = 0, \tag{7}$$

where

$$\frac{\partial G_N}{\partial x_n} = \frac{1}{2\pi\varpi}\delta(\varpi) \quad \text{at } x_n = 0. \tag{8}$$

To solve Eq. (7), we put

$$G_N(x_n, \varpi) = 2\pi \int_0^\infty \hat{G}_N(x_n, k) k J_0(k\varpi)\, \mathrm{d}k, \tag{9}$$

where J_0 is the Bessel function of zero order. Then [27]

$$\frac{\partial^2 \hat{G}_N}{\partial x_n^2} + \frac{2k^2}{a}\left[x_n + \frac{a}{2}\left(\frac{k_o^2}{k^2} - 1\right)\right]\hat{G}_N = 0, \quad x_n > 0 \quad \text{where } \frac{\partial \hat{G}_N}{\partial x_n} = \frac{1}{(2\pi)^2}, \quad x_n = 0. \tag{10}$$

The solution with *outgoing* wave behaviour is [24,25]

$$\hat{G}_N(x_n, k) = \frac{\mathrm{e}^{\mathrm{i}\pi/3}\mathrm{Ai}\left\{\left(\frac{2k^2}{a}\right)^{1/3}\mathrm{e}^{-\mathrm{i}\pi/3}\left[x_n + \frac{a}{2}\left(\frac{k_o^2}{k^2} - 1\right)\right]\right\}}{(2\pi)^2\left(\frac{2k^2}{a}\right)^{1/3}\mathrm{Ai}'\left\{\left(\frac{ka}{2}\right)^{2/3}\mathrm{e}^{-\mathrm{i}\pi/3}\left(\frac{k_o^2}{k^2} - 1\right)\right\}}, \tag{11}$$

where Ai denotes the Airy function [28] and the prime denotes differentiation with respect to the argument.

Putting $x_n = 0$ on the surface, we then find from Eq. (9) that

$$G_N(0,\varpi) = \frac{e^{i\pi/3}}{2\pi}\int_0^\infty \frac{kJ_0(k\varpi)\mathrm{Ai}\left\{e^{-i\pi/3}\left(\frac{ka}{2}\right)^{2/3}\left(\frac{k_o^2}{k^2}-1\right)\right\}dk}{\left(\frac{2k^2}{a}\right)^{1/3}\mathrm{Ai}'\left\{e^{-i\pi/3}\left(\frac{ka}{2}\right)^{2/3}\left(\frac{k_o^2}{k^2}-1\right)\right\}}. \tag{12}$$

When $k_o a \gg 1$ the Bessel function may be replaced by its large argument approximation ($J_0(x)\sim(2/\pi x)^{1/2}\cos(x-\pi/4)$ [28]), and the range of integration extended to $-\infty<k<\infty$, to give

$$G_N(0,\varpi) \approx \frac{e^{i\pi/3}}{(2\pi)^{3/2}\sqrt{\varpi}}\int_{-\infty}^\infty \frac{\sqrt{k+i\varepsilon}\,\mathrm{Ai}\left\{e^{-i\pi/3}\left(\frac{|k|a}{2}\right)^{2/3}\left(\frac{k_o^2}{k^2}-1\right)\right\}e^{i(k\varpi-(\pi/4))}\,dk}{\left(\frac{2|k|^2}{a}\right)^{1/3}\mathrm{Ai}'\left\{e^{-i\pi/3}\left(\frac{|k|a}{2}\right)^{2/3}\left(\frac{k_o^2}{k^2}-1\right)\right\}}, \tag{13}$$

where $\varepsilon\to+0$ and $|k|=\sqrt{k^2+\varepsilon^2}$, with the branch cuts for $\sqrt{k\pm i\varepsilon}$ taken, respectively, from $\mp i\varepsilon$ to $\mp i\infty$ in the k-plane.

As $k_o\varpi\to\infty$ the main contribution to the integral is from the residues of poles in the upper k-plane. These poles are determined by the zeros $\xi=-\sigma_n, n=1,2,3,\ldots$ of $\mathrm{Ai}'(\xi)$, which are real and negative and given by [28]

$$\sigma_1 = 1.01879,\quad \sigma_2 = 3.24820,\quad \sigma_3 = 4.82010,\quad \sigma_n = \left[\frac{3\pi}{8}(4n-3)\right]^{2/3},\ \ n>3. \tag{14}$$

Each σ_n determines a corresponding pole k_n; the functional dependencies of the real and imaginary parts of k_n/k_o on $k_o a/\sigma_n^{3/2}$ are plotted in Fig. 4 (———). It is seen that $\mathrm{Re}(k_n)\sim k_o$ when $k_o a/\sigma_n^{3/2}$ exceeds about 2; it decreases to zero at $k_o a/\sigma_n^{3/2} = 4/3\sqrt{3}\sim 0.77$, below which $\mathrm{Re}(k_n)\equiv 0$, and $\mathrm{Im}(k_n/k_o)$ increases rapidly to $+\infty$ (from $\mathrm{Im}(k_n/k_o)=\sqrt{2}$ at $k_o a/\sigma_n^{3/2} = 4/3\sqrt{3}$). Also shown in the figure (– – –) are the asymptotic dependencies for $k_o a\gg 1$, given by

$$k_n \sim k_o\left[1+\frac{\sigma_n}{2}\left(\frac{2}{k_o a}\right)^{2/3}e^{i\pi/3}\right]. \tag{15}$$

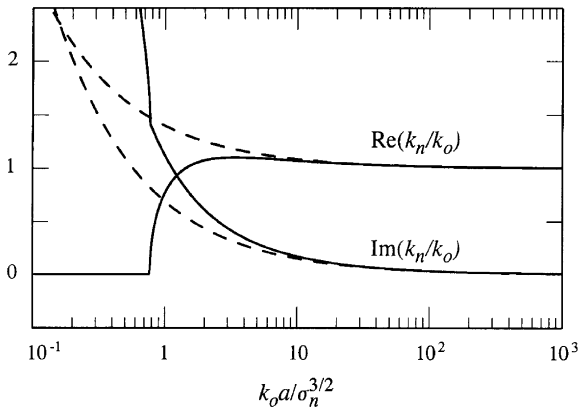

Fig. 4. Dependence on $k_o a/\sigma_n^{3/2}$ of the real and imaginary parts (———) of the pole k_n/k_o of the integrand (13); (– – –) the asymptotic approximation (15).

In terms of these quantities we obtain from Eq. (13) (using the relation $\mathrm{Ai}''(\xi)=\xi\mathrm{Ai}(\xi)$)

$$G_{\mathrm{N}}(0,\varpi)\approx\frac{3\mathrm{e}^{11\mathrm{i}\pi/12}}{2^{2/3}\sqrt{2\pi\varpi a}}\sum_n\frac{(k_na)^{1/6}\mathrm{e}^{\mathrm{i}k_n\varpi}}{\sigma_n\left(\dfrac{2k_o^2}{k_n^2}+1\right)},\quad k_oa\gg1. \tag{16}$$

This formula is to be used to determine the creeping wave approximation to the waves incident on the edge A of the cavitator, where $\varpi=\pi a/2$. However, Pekeris [20] has shown that the accuracy of the earth-flattening approximation (7) degrades rapidly when ϖ exceeds about $\frac{1}{2}a$. The complex phase $k_n\varpi$ is well predicted, but the amplitude factor $1/\sqrt{\varpi}$ *overestimates* the decrease in creeping wave amplitude with distance over the surface of the hemisphere.

This defect is corrected by appeal to the geometrical theory of diffraction [23,25], according to which the creeping wave amplitude is inversely proportional to the square root of the (circumferential) length Λ of the wavefront on S_{N}. Now $\Lambda=2\pi r(\varpi)$, where $r(\varpi)$ is the radial distance to S_{N} indicated in Fig. 3 from the axis of symmetry. Therefore, because $\varpi\approx r(\varpi)$ when ϖ/a is small, the appropriate correction is obtained by replacing ϖ in the denominator of the right-hand side of Eq. (16) by $r(\varpi)$, yielding

$$G_{\mathrm{N}}(0,\varpi)\approx\frac{3\mathrm{e}^{11\mathrm{i}\pi/12}}{2^{2/3}\sqrt{2\pi ar(\varpi)}}\sum_n\frac{(k_na)^{1/6}\mathrm{e}^{\mathrm{i}k_n\varpi}}{\sigma_n\left(\dfrac{2k_o^2}{k_n^2}+1\right)},\quad k_oa\gg1. \tag{17}$$

3.2. Diffraction at the edge of the cavitator

The creeping surface wave (17) is diffracted further at the edge A of the cavitator, across which the surface condition changes from $\partial G/\partial x_n=0$ to $G=0$. Near the edge A ($r(\varpi)\to a$) the wave $G_{\mathrm{N}}(0,\varpi)$ consists of a slowly varying amplitude $\times\,\mathrm{e}^{\mathrm{i}k_o\varpi}$. The cavity interface $r=a$ is the tangential, circular cylindrical continuation of the circular edge A, parallel to the x-axis. To calculate the edge diffraction we replace the cavitator by a *rigid* upstream continuation of this cylinder (indicated by the broken lines in Fig. 3). We then regard the creeping wave (17) as being incident on A from along this rigid cylinder, and put

$$G_{\mathrm{N}}(0,\varpi)=\mathscr{G}_{\mathrm{I}}\,\mathrm{e}^{\mathrm{i}k_ox}, \tag{18}$$

where

$$\mathscr{G}_{\mathrm{I}}=\frac{3\mathrm{e}^{11i\pi/12}}{2^{2/3}\sqrt{2\pi a}}\sum_n\frac{(k_na)^{1/6}\,\mathrm{e}^{\mathrm{i}k_n\ell}}{\sigma_n\left(\dfrac{2k_o^2}{k_n^2}+1\right)},\quad \ell=\frac{\pi a}{2}. \tag{19}$$

Then, if G_{S} denotes the edge diffracted component of G we can write in the region $r>a$

$$G=\mathscr{G}_{\mathrm{I}}\,\mathrm{e}^{\mathrm{i}k_ox}+G_{\mathrm{S}}(x,r), \tag{20}$$

wherein for some suitable $\mathscr{A}(k)$ we can put [10,17,29]

$$G_{\mathrm{S}}(x,r)=\int_{-\infty}^{\infty}\mathscr{A}(k)H_0^{(1)}(\gamma r)\,\mathrm{e}^{\mathrm{i}kx}\,\mathrm{d}k, \tag{21}$$

where $H_0^{(1)}$ is the zero order Hankel function and $\gamma=\sqrt{k_o^2-k^2}$, with branch cuts in the k-plane extending from $k=\pm(k_o+\mathrm{i}0)$ to $\pm\mathrm{i}\infty$, so that γ is positive imaginary on the real axis when $|k|>k_o$.

The kernel function $\mathscr{A}(k)$ is determined from the conditions

$$\left.\begin{array}{ll}\dfrac{\partial G}{\partial r}=0, & x<0\\ G=0, & x>0\end{array}\right\},\quad r=a+0, \tag{22}$$

which supply the following dual integral equations satisfied by $\mathscr{A}(k)$:

$$\int_{-\infty}^{\infty} \gamma \mathscr{A}(k) H_1^{(1)}(\gamma a)\, \mathrm{e}^{\mathrm{i}kx}\, \mathrm{d}k = 0, \quad x<0, \tag{23}$$

$$\int_{-\infty}^{\infty} \left(\mathscr{A}(k) H_0^{(1)}(\gamma a) + \frac{\mathscr{G}_{\mathrm{I}}}{2\pi \mathrm{i}(k-k_o-\mathrm{i}0)} \right) \mathrm{e}^{\mathrm{i}kx}\, \mathrm{d}k = 0, \quad x>0. \tag{24}$$

In these integrals the Hankel functions $H_0^{(1)}, H_1^{(1)}$ may be replaced by their large argument approximations [28] when $k_o a \gg 1$. The equations are then readily solved by the Wiener–Hopf procedure, yielding for the solution G that remains finite at A

$$G(x,r) \approx \mathscr{G}_{\mathrm{I}} \left(\mathrm{e}^{\mathrm{i}k_o x} + \frac{i}{\pi} \sqrt{\frac{k_o a}{2r}} \int_{-\infty}^{\infty} \frac{\mathrm{e}^{\mathrm{i}\{kx+\gamma(r-a)\}}\, \mathrm{d}k}{\sqrt{k_0+k}(k-k_o-\mathrm{i}0)} \right), \quad k_o a \gg 1 \tag{25}$$

(see [29,30] for details).

Hence, at distance $x>0$ from the cavitator edge A on the cavity interface

$$\frac{\partial G}{\partial r} \approx \mathscr{G}_{\mathrm{I}} \sqrt{\frac{2k_o}{\pi x}}\, \mathrm{e}^{\mathrm{i}(k_o x - \pi/4)}, \quad k_o a \gg 1. \tag{26}$$

Using formula (19) and definition (6), this provides the following explicit formula for the transfer function:

$$T(x,\omega) \approx -\frac{1}{2^{2/3}\pi a^2} \sqrt{\frac{k_o a}{x/a}} \left(3 \sum_n \frac{(k_n a)^{1/6}\, \mathrm{e}^{\mathrm{i}k_n' \ell}}{\sigma_n \left(\dfrac{2k_o^2}{k_n^2} + 1 \right)} \right) \mathrm{e}^{\mathrm{i}(k_o(\ell+x)+2\pi/3)}, \quad k_o a \gg 1, \tag{27}$$

where $k_n' = k_n - k_o$.

4. The transfer function at low and intermediate frequencies

4.1. The hydrodynamic approximation

The behaviour of $T(x,\omega)$ at very low frequencies is determined by the solution of Eqs. (3) and (4) in the hydrodynamic limit in which $k_o a \to 0$. An understanding of this limiting behaviour (when the local flow produced by the source at N resembles that of an incompressible fluid) is useful for mapping out the properties of the transfer function over the whole frequency range, and not just in the high-frequency approximation of Section 3. The precise geometry of the nose should not be important in this limit — the important aspect of the problem is contained in the coupling in incompressible flow of the source flow at N with a neighbouring 'pressure release' interface.

A highly simplified model of this situation is illustrated in Fig. 5. Here the cavitator nose has been 'flattened' into a rigid circular disc of radius ℓ in the plane $x_n = 0$, and the cavity interface has been deformed into the infinite region of this plane in $\varpi > \ell$. Green's function satisfies

$$\left(\frac{\partial^2}{\partial x_n^2} + \frac{1}{\varpi} \frac{\partial}{\partial \varpi} \left(\varpi \frac{\partial}{\partial \varpi} \right) \right) G = 0, \quad x_n > 0 \tag{28}$$

with

$$\left.\begin{array}{ll} \dfrac{\partial G}{\partial x_n} = \dfrac{1}{2\pi\varpi}\delta(\varpi), & \varpi < \ell \\ G = 0, & \varpi > \ell \end{array}\right\}, \quad x_n = 0. \tag{29}$$

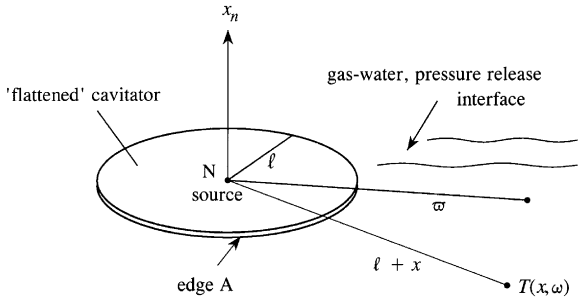

Fig. 5. Sketch of the geometrically 'flattened' analytical model used to estimate the magnitude of the transfer function $T(x,\omega)$ in the low-frequency, hydrodynamic limit $k_o a \to 0$.

This is a standard problem of classical potential theory [31] which is solved by setting

$$G(x_n,\varpi) = \int_0^\infty \mathscr{B}(k) J_0(k\varpi)\, \mathrm{e}^{-kx_n}\, \mathrm{d}k, \tag{30}$$

where $\mathscr{B}(k)$ satisfies the dual system

$$\int_0^\infty k\mathscr{B}(k) J_0(k\varpi)\, \mathrm{d}k = -\frac{1}{2\pi\varpi}\delta(\varpi), \quad \varpi < \ell, \tag{31}$$

$$\int_0^\infty \mathscr{B}(k) J_0(k\varpi)\, \mathrm{d}k = 0, \quad \varpi > \ell. \tag{32}$$

The solution is given by Sneddon ([31, Section 3.5]) in the form

$$\mathscr{B}(k) = -\frac{1}{\pi^2}\int_0^1 \frac{\sin(k\ell\xi)}{\xi}\, \mathrm{d}\xi. \tag{33}$$

This is now used to evaluate the normal derivative $\partial G/\partial r \equiv -T(x,\omega)$ of Eq. (6). In the present deformed geometry the normal derivative corresponds to $\partial G/\partial x_n$, and we readily determine the low-frequency approximation of this derivative by the substitution of Eq. (33) into Eq. (30), which gives

$$T(x,\omega) \sim \frac{\ell}{\pi^2(\ell+x)^2\sqrt{x(2\ell+x)}}, \quad k_o a \to 0. \tag{34}$$

4.2. Approximation for intermediate frequencies

Some idea of the behaviour of the transfer function when $k_o a \sim O(1)$ can be obtained by combining the hydrodynamic approximation of Section 4.1 and the doubly infinite edge diffraction model of Fig. 3.

When the edge of the 'flattened' nose of Fig. 5 is ignored, the surface potential G_{N} produced by the point source at N is given by

$$G_{\mathrm{N}}(0,\varpi) = -\frac{\mathrm{e}^{\mathrm{i}k_o\varpi}}{2\pi\varpi}. \tag{35}$$

We shall take this to represent the field incident on the edge A of the hemispherical cavitator when $k_o a \sim O(1)$, but is too small to justify the use of the creeping wave approximation. The method of Section 3.2 may then be used to determine the influence of diffraction on the incident wave (35) by setting

$$\mathscr{G}_{\mathrm{I}} = -\frac{\mathrm{e}^{\mathrm{i}k_o\ell}}{2\pi\ell} \tag{36}$$

in Eq. (18).

Then (26) yields

$$T(x,\omega)\sim -\frac{1}{2^{1/2}\pi^{3/2}\ell}\sqrt{\frac{k_o}{x}}\mathrm{e}^{\mathrm{i}(k_o(\ell+x)-(\pi/4))},\quad k_oa\sim O(1). \tag{37}$$

5. Numerical results

5.1. The transfer function

The transfer function $T(x,\omega)$ determines the strength of the self-noise at the nose N in terms of the distributed pressure field p_v of the impinging ventilating gas, in accordance with Eq. (5). To illustrate its frequency dependence we shall consider the non-dimensional quantity $a^2|T(x,\omega)|$.

At high frequencies this is governed by the creeping wave approximation (27). In that formula $\ell=(\pi/2)a$. Now it is readily verified from Eq. (14) and the results displayed in Fig. 4, that only the first term in the residue expansion in terms of the poles k_n is important for $k_oa\geqslant 1$. For example, the ratio of the absolute values of the second to the first term in the expansion decreases rapidly from $\sim$0.03 when k_oa increases from $k_oa=1$.

For $k_oa>1$ we shall therefore take

$$a^2|T(x,\omega)|\approx\frac{3}{2^{2/3}\pi}\sqrt{\frac{a}{x}}(k_oa)^{1/2}\left|\frac{(k_1a)^{1/6}\,\mathrm{e}^{\mathrm{i}k_1'(\pi/2)a}}{\sigma_1\left(\dfrac{2k_o^2}{k_1^2}+1\right)}\right|. \tag{38}$$

This approximation is plotted as the 'creeping wave' curve in Fig. 6 for $x=2a$, i.e. at one cavity diameter downstream of the edge A of the cavitator. The straight line labelled 'flat nose' also plotted in the figure represents the corresponding low-frequency prediction from formula (37), which would arguably be expected to furnish an over estimate of the actual level at the nose. It seems reasonable, therefore, to connect these high- and low-frequency limiting behaviours by means of the smooth, broken-line interpolating curve shown in the figure. The level of the predicted 'hydrodynamic limit' ($k_oa=0$) is also indicated in the figure. It is evidently attained in practice only at very low frequencies.

Fig. 7 shows how the acoustic levels are only marginally decreased when $x=4a$. The hydrodynamic level is reduced by about 17 dB, because of the relative rapid fall-off with distance of hydrodynamic motions interacting with the cavitator edge and the cavity interface.

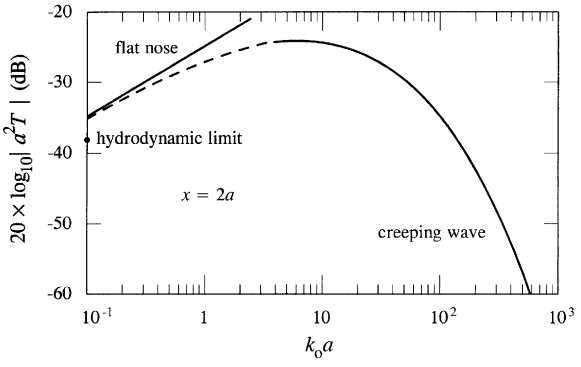

Fig. 6. The creeping wave and low-frequency ('flat nose') approximations (———) for $20\log_{10}(a^2|T|)$ (dB) at $x=2a$; the broken line curve represents a possible interpolation between these limits.

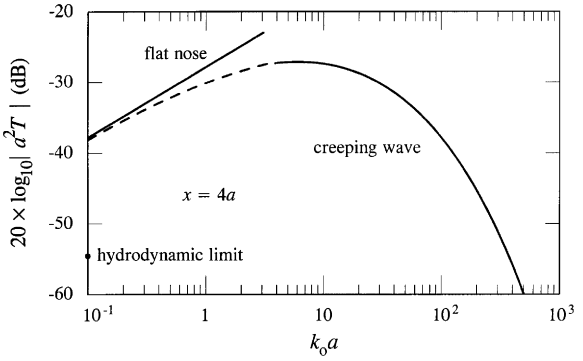

Fig. 7. The creeping wave and low-frequency ('flat nose') approximations (———) for $20\log_{10}(a^2|T|)$ (dB) at $x = 4a$; the broken line curve represents a possible interpolation between these limits.

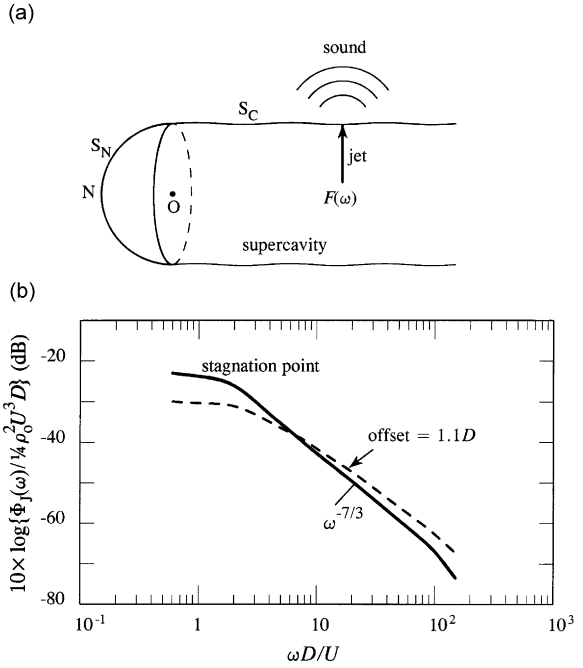

Fig. 8. (a) Sound generation by a jet impinging on the gas–water interface S_C. (b) Stagnation point wall pressure spectrum (———) measured by Strong et al. [32] for a turbulent air jet of mean density ρ_o impinging at normal incidence on a plane wall. The jet exhausts at speed $U = 136\,\text{ft/s}$ from a round nozzle of diameter $D = \frac{1}{3}\,\text{ft}$; the nozzle exit plane is distance $7D$ from the wall. (– – –) wall pressure spectrum at an offset of $1.1D$ from the jet centreline.

5.2. *Self-noise produced by an impinging gas jet*

A practical illustration of the level of the predicted self-noise at the nose can be gained by considering the sound generated by the normal impingement on the cavity wall S_C of an unsteady circular gas jet. If the jet radius is small compared to the acoustic wavelengths of interest, the impact of the jet with the interface is dynamically equivalent to the application of a radial surface force $F(\omega)$ (in the direction of increasing r) at a point on the interface, and Eq. (5) then reduces to

$$p_N(\omega) = T(x,\omega)F(\omega), \tag{39}$$

where x denotes the distance from the cavitator edge of the point of intersection of the interface and the jet axis (Fig. 8a).

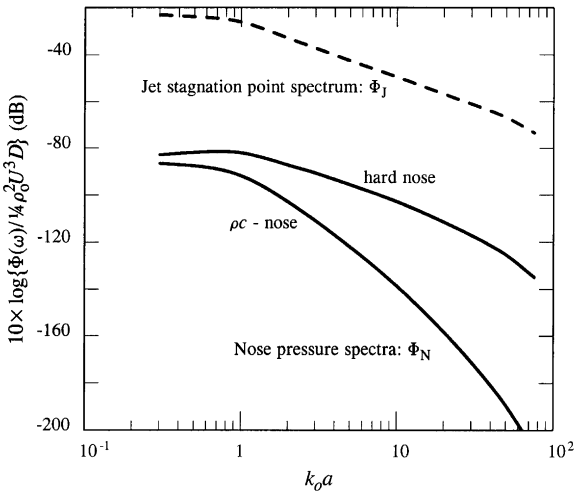

Fig. 9. The predicted self-noise nose pressure spectrum $10\log_{10}\{\Phi_N(\omega)/\frac{1}{4}\rho_o^2U^3D\}$ calculated from Eq. (39), attributable to an air jet exhausting at speed $U=40\,\mathrm{m/s}$ from a round nozzle of diameter $D=1.6\,\mathrm{mm}$ at distance $7D$ from the cavity interface when $x=2a, a=30\,\mathrm{mm}$, and when the jet stagnation point pressure spectrum $\Phi_J(\omega)$ corresponds to that measured by Strong et al. [32]. The case of a cavitator with a ρc-nose is discussed in Section 6.

Because of the large density difference between the cavity interior gas and the water, Foley et al. [14] argued that the overall jet normal force $F(\omega)$ could be identified with the force that would be exerted on the interface when the latter is assumed to be *rigid*. Small scale turbulence in the water produced by the impact can exert no additional net force on the interface, and its accumulation in the vicinity of the jet impingement zone is, in any event, inhibited because it is swept downstream in the hydrodynamic mean flow. Therefore, in a first approximation measurements of the surface force produced by a jet impinging on a rigid wall can be used to estimate the self-noise at the nose.

The solid curve in Fig. 8b represents the wall pressure spectrum $\Phi_J(\omega)$ measured by Strong et al. [32] on the centreline of a round air jet impinging normally on a plane wall. The jet exhausts at speed $U=136\,\mathrm{ft/s}$ from a nozzle of diameter $D=\frac{1}{3}$ ft whose exit plane is distance $7D$ from the wall; the centreline of the jet meets the wall at a stagnation point. To determine the net normal force it is necessary to know the correlation properties of the surface pressure across the impact region. This data is not available in the published measurements. However, also shown in Fig. 8b (– – –) is the wall pressure spectrum measured at a radial offset of $1.1D$ from the stagnation point. The differences between the spectra in the important higher range of frequencies ($\omega D/U>2$) are sufficiently small to justify the assumption that the force pressure spectrum (which is proportional to $|F(\omega)|^2$) can be approximated by $\mathscr{A}_J^2\Phi_J(\omega)$, where $\mathscr{A}_J\equiv(\pi/4)d^2$ is an effective impact area of the jet of diameter d.

Eq. (39) then implies that the pressure spectrum at the nose $\Phi_N(\omega)$, say, is given by

$$\Phi_N(\omega)=\mathscr{A}_J^2|T(x,\omega)|^2\Phi_J(\omega), \tag{40}$$

when the jet nozzle-interface distance $\sim 7D$. If we assume that the jet diverges conically with a total angular width of $\sim 25^\circ$ [16], it follows that $d\sim D+3D$.

The corresponding prediction of the nose pressure spectrum $\Phi_N(\omega)$ produced by a single jet is plotted in Fig. 9 (the curve labelled 'hard nose') for $D=0.0625\,\mathrm{in}\sim 1.6\,\mathrm{mm}$, $d=6.4\,\mathrm{mm}$, when $U=40\,\mathrm{m/s}$ and for a supercavity of radius $a=30\,\mathrm{mm}$. Over the broad range of central frequencies ($1<k_oa<10^2$) the transfer function varies by only a few dB from its maximum near $k_oa\sim 8$. Therefore the shape of the nose pressure spectrum is similar to the stagnation point pressure spectrum (also shown in the figure), slightly depressed by a few dB at the frequency extremes but otherwise uniformly smaller by about 50 dB. The overall level of the nose pressure spectrum would be raised uniformly by $10\log_{10}N\,\mathrm{dB}$ in the more general case involving an array of N mutually independent turbulent jets impinging on the cavity interface.

6. Conclusion

The approximate representation of the transfer function derived in this paper determines directly the level of self-noise at the cavitator nose produced by ventilating gas impinging on the gas–water, supercavity interface. This can be used to provide a complete estimate of the noise produced by the annular array of jets used to maintain the specially constructed ARL experimental supercavity discussed in Section 1. To do this it will first be necessary to determine the spectra of the cavity wall impact forces produced by the jets, in a first approximation by the method of Section 5.2, where the force is assumed to be the same as that produced by impingement on a rigid wall. This procedure should be adequate provided the jet diameter at impact is smaller than the smallest acoustic wavelength of interest, otherwise it will be necessary to measure the detailed properties of the impinging pressure field across the jet at the interface.

The detailed formulae given in this paper are for the particular case of an acoustically hard nose. Similar results are easily obtained by the same method with minor changes in the formalisms when the surface motions satisfy a general impedance boundary condition [21–26]. For example, the curve in Fig. 9 labelled 'ρc-nose' illustrates the large reductions in the predicted self-noise that are achieved when the hemispherical cavitator is compliant, the case shown being for a locally reacting surface with impedance equal to $\rho_o c_o$.

Acknowledgements

The work reported here is sponsored by the Office of Naval Research Code 333, Grant N00014-06-1-0270 under the University/Laboratory Initiative directed by Dr. Kam W. Ng. A.M.C. was supported by a Boston University Undergraduate Research Assistantship.

References

[1] R. Kuklinski, C. Henoch, J. Castano, Experimental study of ventilated cavities on dynamic test model, Paper presented at *Cav*2001: *Session* B3.004, 2001.
[2] J.P. Franc, J.M. Michel, *Fundamentals of Cavitation*, Kluwer Academic Publishers, Dordrecht, 2004.
[3] C.E. Brennen, *Cavitation and Bubble Dynamics*, Oxford University Press, Oxford, 1995.
[4] E. Silberman, C.S. Song, Instability of ventilated cavities, *Journal of Ship Research* 5 (1) (1961) 13–33.
[5] C.S. Song, Pulsation of ventilated cavities, *Journal of Ship Research* 5 (4) (1962) 8–20.
[6] M.J. Lighthill, On sound generated aerodynamically. Part I: general theory, *Proceedings of the Royal Society of London A* 211 (1952) 564–587.
[7] J.E. Ffowcs Williams, Hydrodynamic noise, *Annual Review of Fluid Mechanics* 1 (1969) 197–222.
[8] D.G. Crighton, Basic principles of aerodynamic noise generation, *Progress in Aerospace Sciences* 16 (1975) 31–96.
[9] W.K. Blake, *Mechanics of Flow-induced Sound and Vibration*, Academic Press, New York, 1986.
[10] M.S. Howe, *Acoustics of Fluid–Structure Interactions*, Cambridge University Press, Cambridge, 1998.
[11] M.S. Howe, *Theory of Vortex Sound*, Cambridge University Press, Cambridge, 2003.
[12] S.D. Young, T.A. Brungart, G.C. Lauchle, M.S. Howe, Effect of a downstream ventilated gas cavity on the spectrum of turbulent boundary layer wall pressure fluctuations, *Journal of the Acoustical Society of America* 118 (2005) 3506–3512.
[13] A.W. Foley, M.S. Howe, T.A. Brungart, Sound generated by a jet-excited spherical cavity, *Journal of Sound and Vibration* 315 (2008) 88–99.
[14] A.W. Foley, M.S. Howe, T.A. Brungart, Sound generated by gas-jet impingement on the interface of a supercavity, *Proceedings of IMECE2008, 2008 ASME International Mechanical Engineering Congress*, Boston, MA, USA, November 2–6, 2008.
[15] B.B. Baker, E.T. Copson, *The Mathematical Theory of Huygens' Principle*, second ed., Oxford University Press, Oxford, 1969.
[16] L.D. Landau, E.M. Lifshitz, *Fluid Mechanics*, second ed., Pergamon, Oxford, 1987.
[17] D.G. Crighton, A.P. Dowling, J.E. Ffowcs Williams, M. Heckl, F.G. Leppington, *Modern Methods in Analytical Acoustics (Lecture Notes)*, Springer, London, 1992.
[18] G.N. Watson, The diffraction of electric waves by the Earth, *Proceedings of the Royal Society of London A* 95 (1919) 83–99.
[19] J.C. Schelleng, C.R. Burrows, E.B. Ferrell, Ultra-short-wave propagation, *Proceedings of the Institute of Radio Engineers* 21 (1933) 427–463.
[20] C.L. Pekeris, Accuracy of the earth-flattening approximation in the theory of microwave propagation, *Physical Review* 70 (1946) 518–522.
[21] D.E. Kerr (Ed.), *Propagation of short radio waves*, Radiation Laboratory Report 13, Massachusetts Institute of Technology, 1947.
[22] B. Friedman, Propagation in a non-homogeneous atmosphere, *Proceedings of the Theory of Electromagnetic Waves*, New York, Interscience, New York, June 6–8, 1951, pp. 317–350.

[23] B.R. Levy, J.B. Keller, Diffraction by a smooth object, *Communications on Pure and Applied Mathematics* 12 (1959) 159–209.
[24] K.G. Budden, *The Wave-guide Mode Theory of Wave Propagation*, Logos Press, London, 1961.
[25] A.D. Pierce, *Acoustics, An Introduction to its Principles and Applications*, American Institute of Physics, New York, 1989.
[26] M.C. Junger, D. Feit, *Sound, Structures and their Interactions*, Acoustical Society of America, New York, 1993.
[27] I.N. Sneddon, *The Use of Integral Transforms*, McGraw-Hill, New York, 1972.
[28] M. Abramowitz, I.A. Stegun (Eds.), *Handbook of Mathematical Functions*, Ninth corrected printing, US Department of Commerce, National Bureau of Standards Applied Mathematics Series No. 55, Washington, DC, 1970.
[29] B. Noble, *Methods Based on the Wiener–Hopf Technique*, Pergamon Press, London, 1958.
[30] P.C. Clemmow, *The Plane Wave Spectrum Representation of Electromagnetic Fields*, Pergamon Press, London, 1966.
[31] I.N. Sneddon, *Mixed Boundary Value Problems in Potential Theory*, North-Holland, Amsterdam, 1966.
[32] D.R. Strong, T.E. Siddon, W.T. Chu, *Pressure fluctuations on a flat plate with oblique jet impingement*, Contractor Report NASA CR-839, National Aeronautics and Space Administration, 1967.